NOTES AND CORRESPONDENCE

In Situ Atmospheric Turbulence Measurement Using the Terrestrial Magnetic Field— A Compass for a Radiosonde

R. Giles Harrison and Robin J. Hogan

Department of Meteorology, University of Reading, Reading, United Kingdom

ABSTRACT

A method for in situ detection of atmospheric turbulence has been developed using an inexpensive sensor carried within a conventional meteorological radiosonde. The sensor—a Hall effect magnetometer—was used to monitor the terrestrial magnetic field. Rapid time scale (10 s or less) fluctuations in the magnetic field measurement were related to the motion of the radiosonde, which was strongly influenced by atmospheric turbulence. Comparison with cloud radar measurements showed turbulence in regions where rapid time-scale magnetic fluctuations occurred. Reliable measurements were obtained between the surface and the stratosphere.

1. Introduction

Identification and prediction of atmospheric turbulence are important because of the associated severe aviation hazards. Turbulence permits the efficient transfer of heat, moisture, and momentum, and its understanding is central to prediction and understanding of clouds and weather systems. Characterization of vertical diffusion caused by turbulence is also an important parameter for numerical weather forecast models and the dispersion of pollutants and other atmospheric gases. A new sensing technique for in situ measurement of atmospheric turbulence is described here.

The technique uses a Hall effect magnetic field sensor, carried on a standard Vaisala RS80 meteorological radiosonde. The Hall sensor chosen responds rapidly to small magnetic fields, and is sufficiently sensitive to detect the terrestrial magnetic field, which is ~45 μT parallel to the field lines at 52°N (MacGorman and Rust 1998). The terrestrial magnetic field is relatively stable, with differences between two antipodal measurements changing by less than 50 nT since 1868 (Maynaud 1972). Turbulent atmospheric motions produce fluctuations in

the radiosonde's motion, and change the Hall sensor's orientation with respect to the terrestrial magnetic field. The radiosonde Hall sensor's output voltage therefore varies with the motion of the radiosonde, and fluctuations in the sensor's output primarily result from local atmospheric turbulence modulating the position of the Hall sensor. Other sources of magnetic variability are negligible: the in-cloud magnetic field (MacGorman and Rust 1998) is typically a factor of 2000 smaller.

The Hall sensor is inexpensive and does not require calibration; this is a cost-effective aspect as the radiosonde is lost after the ascent. Further, the absence of moving parts ensures reliability even in the presence of ice. Essentially the sensor contributes a sensitive high time-resolution compass to a standard radiosonde.

The Hall sensor measurements are telemetered to the ground over the radiosonde's UHF radiolink, using a temperature-stable digital data acquisition system (Harrison 2005).

2. Hall sensor electronics

The magnetic field sensing system is based on a Honeywell SS495 linear ratiometric Hall effect sensor, which is a small magnetic field sensor in a transistor-sized (4 mm × 3 mm) plastic package. It is a laser-trimmed device having a magnetic sensitivity of (3.125 ± 0.125) mV (100 μT)$^{-1}$ without further calibration,

Corresponding author address: Dr. Robin Hogan, Dept. of Meteorology, University of Reading, P.O. Box 243, Earley Gate, Reading RG6 6BB, United Kingdom.
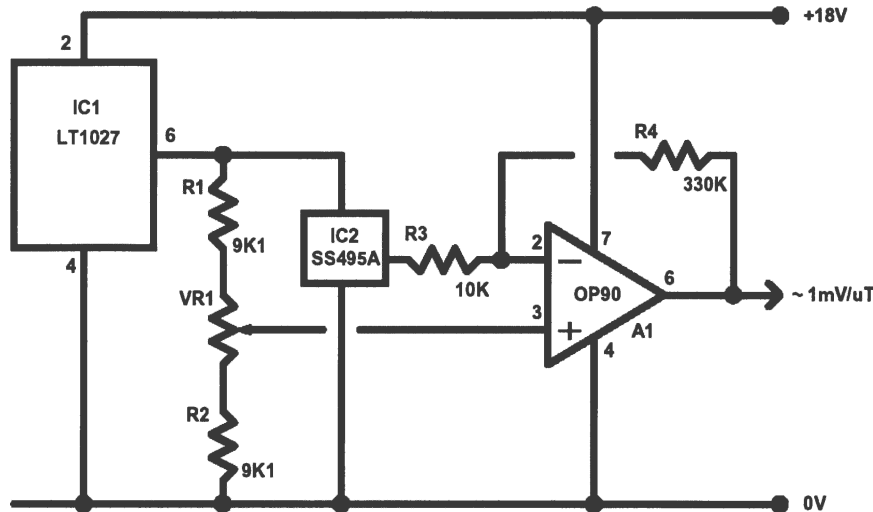E-mail: r.j.hogan@reading.ac.uk

FIG. 1. Circuit diagram of Hall sensor signal conditioning electronics. [Components: IC1 LT1027 3 ppm $(\degree C)^{-1}$ 5.000-V voltage reference; IC2 SS495A Hall effect sensor; A1 OP90 micropower opamp; R1 and R2 9.1 kΩ, R3 10 kΩ, R4 330 kΩ metal film 15 ppm $(\degree C)^{-1}$ resistors; VR1 1 kΩ 100 ppm $(\degree C)^{-1}$ 12-turn trimmer.]

when operated from a 5-V supply. The SS495 has good temperature stability of sensitivity [-0.01% $(\degree C)^{-1}$] and offset [$\pm 0.07\%$ $(\degree C)^{-1}$], and is specified to operate down to $-40\degree C$. To extract the small changes in the magnetic field, some additional signal processing electronics were added. This consisted of a stable voltage reference, and an amplifying stage to increase the output to nominally 1 mV/μT. This gain was chosen so that, for the horizontal component of the terrestrial magnetic field of ~30 μT, rotating the sensor in the horizontal plane produced a fluctuation of ± 30 mV, which was about 10 times larger than the voltage resolution of the radiosonde data acquisition and interface system (Harrison 2005).

Figure 1 shows a schematic of the signal conditioning electronics used with the SS495 Hall sensor. IC1 is an ultrastable [3 ppm $(\degree C^{-1})$] 5.000-V voltage reference used to provide a temperate stable excitation to the Hall sensor. The output of the Hall sensor is centered on 2.5 V, with positive and negative deviations from 2.5 V depending on the magnetic field alignment. To test the system, a large solenoid coil of 157 turns (length, 59.5 cm; diameter, 18.5 cm) was used to generate a magnetic field, with the Hall sensor mounted within the coil. Using currents spanning ± 2.8 A, and adjusting the sensor's position for maximum output, the Hall sensor response was found to be highly linear, with a sensitivity of 0.03 mV/μT. This is at the lower limit of the manufacturer's specified sensitivity.

A unipolar voltage input (ranging over 0 to +5V) is required by the radiosonde data acquisition interface.

Using a single opamp stage based on A1, the Hall sensor output is offset from its central 2.5 V by the adjustable potential divider formed by R1-VR1-R2. A gain of -33 (set by the ratio R4/R3) is then applied, raising the output to nominally 1 mV/μT. VR1 was adjusted to provide an average output voltage, after the gain stage, of about 2.5 V, to keep the signal voltage within the interface input voltage range despite thermal drift in flight. The power supply for the circuit (+18 V) was provided by the radiosonde interface from the radiosonde's wet battery: the additional current required by this sensor circuit is less than 10 mA, negligible in comparison with the current required by the radio transmitter.

The output voltage from the sensor was sampled using a 12-bit analog-to-digital converter, controlled by a programmed microcontroller within the radiosonde interface. The microcontroller sampled the Hall sensor voltage at an average rate of 3 Hz for 20 s, before the program made self-calibration checks for 2 s. (The actual sampling rate achieved, measured over 1 h, was 2.88 Hz.) Higher sampling rates are possible, at up to about 10 Hz, but the greater rates require some data compression rather than the plain ASCII transmission method used.

The sensor and signal conditioning electronics of Fig. 1 were constructed on a small (12 mm $\times$ 40 mm) circuit board, mounted within an RS80 radiosonde with the Hall sensor's axis mounted to detect the horizontal component of the terrestrial magnetic field. The sensor electronics contributed 6 g of the total 252 g mass of the
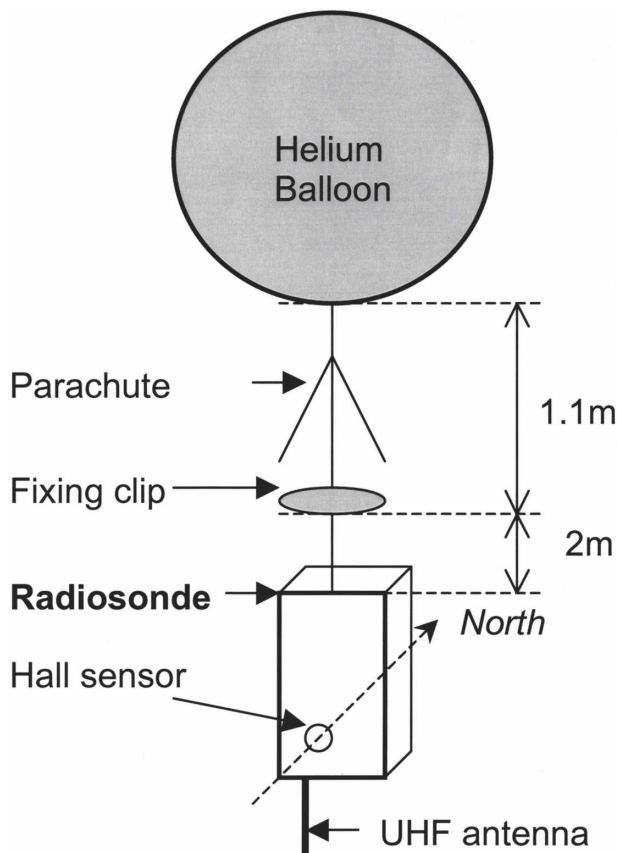
FIG. 2. Schematic (not to scale) of the radiosonde flight train, illustrating the position of the Hall sensor within the radiosonde and the direction of the horizontal magnetic sensing axis (more positive output voltages correspond to northerly directions). Dimensions of the RS80 radiosonde are 95 mm wide × 145 mm high × 60 mm deep.

radiosonde, interface, and sensor. Figure 2 shows the position of the sensor within the radiosonde, together with the flight train between the radiosonde and the balloon.

3. Results

An atmospheric ascent was made from Reading, United Kingdom, on 26 January 2004, using the Hall sensor mounted inside an RS80 radiosonde, carried by a 100-g helium-filled balloon. During this ascent, turbulence parameters were sensed remotely using the Chilbolton 94-GHz Galileo cloud radar, 50 km southwest of Reading, which were compared with the geomagnetic measurements from the Hall sensor.

Figure 3a shows a time series of the data obtained from the radiosonde, following its launch at 1638 UTC. The time series shows rapid magnetic field fluctuations, as well as a steady drift in the mean level of the sensor

voltage. The rapid fluctuations are due to the rotation or swing of the radiosonde, but the drift is closely related to the change in the temperature of the radiosonde's electronic enclosure, showing that the temperature compensation of the sensor is inadequate for absolute magnetometry without further temperature correction. The thermal drift is, however, sufficiently slow that it can be removed by a linear regression to allow the more rapid fluctuations to be extracted. For the meteorological application envisaged, the rapid response is more important than the absolute accuracy, and therefore some thermal instability can be tolerated.

Figure 3b shows the drift-corrected Hall signal, calibrated to magnetic field B using the Honeywell sensor's data sheet calibration. The vertical height is also shown, derived by combining the pressure and temperature measurements of the radiosonde to calculate the atmospheric density, and summing the layer thickness between samples. Approximate descriptions of the atmospheric regions have been added, based on the cloud radar and meteorological profiles presented later (Figs. 5 and 6). Following the drift correction, it is clear that the magnetic field sensor responds to positive and negative B, as would be expected from rotation of the radiosonde and sensor. Because of the rapid response of the Hall sensor to changes in position, the variations are likely to arise from the motions of the radiosonde.

Figure 3c shows a short period of the detrended data, about 1000 s after launch, with a moving average added. The positive and negative variations confirm that the Hall sensor is rotating about its axis, although the nature of the oscillation is not a simple sinusoid. Both the period and the amplitude of the oscillation vary. Oscillations with time scales of the order of seconds to tens of seconds are present: the spectrally separated slow and more rapid fluctuations present are likely to be primarily due to rotation and swing, respectively, as the period of a simple pendulum, with string length ~2 m, is 2.8 s.

Balloons ascending at subcritical Reynolds number generally take a spiral path (MacCready 1965), with the effect of adding a radiosonde package to modify the coupling between lateral and balloon motion. Should the balloon shape become asymmetric, such as through nonisotropic expansion of the balloon during the flight, this response will change with time. Linear expansion of the balloon during the whole ascent is typically up to a factor of 5 (HMSO 1961).

4. Data analysis

Power spectra from the magnetic field data were derived and are shown in Fig. 4. The spectra were ob-
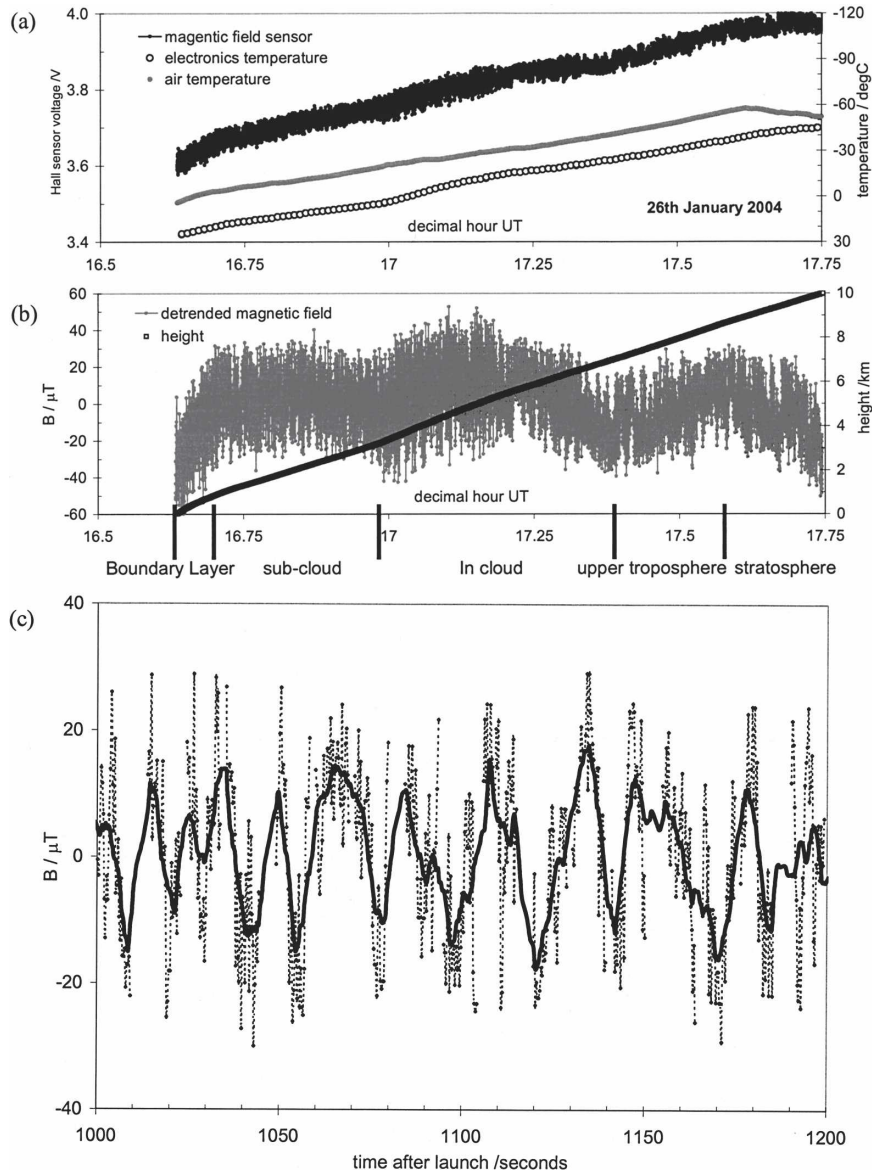
FIG. 3. Time series of data obtained from radiosonde released from Reading at 1638 UTC on 26 Jan. (a) Raw voltage from Hall effect sensor and temperature measurements of the outside air and electronics environment; (b) linearly detrended Hall sensor voltage calibrated to magnetic field and radiosonde height, derived from radiosonde pressure sensor; (c) a period of the detrended data 1000 s after launch, with a 16-s centered moving average added.

tained from short periods of data (100 s), in each of the regions marked in Fig. 3b. Because of the irregular sampling of the magnetic field data, the spectra were derived using the Lomb periodogram (Press et al. 1992). As well as dealing with the irregular sampling without interpolation, this method has the advantage of giving information at frequencies greater than the usual Nyquist cutoff frequency, as the irregular sampling removes ambiguity concerning the frequencies present. It also provides statistical confidence information on the spectral peaks present.

Figure 4 shows that the frequencies present in the magnetic field data are similar in the boundary layer (Fig. 4a), upper troposphere (Fig. 4d), and stratosphere (Fig. 4e), with a common decrease in spectral power from low frequencies to high frequencies. The spectra beneath (Fig. 4b) and within (Fig. 4c) the cloud layer are different, with more energy across the spectra obtained, particularly at frequencies above 0.1 Hz. In moving from the subcloud to in-cloud regions, more power becomes apparent in the frequencies between 0.1 and 1 Hz. Figures 4b, 4c, and 4e show the transition
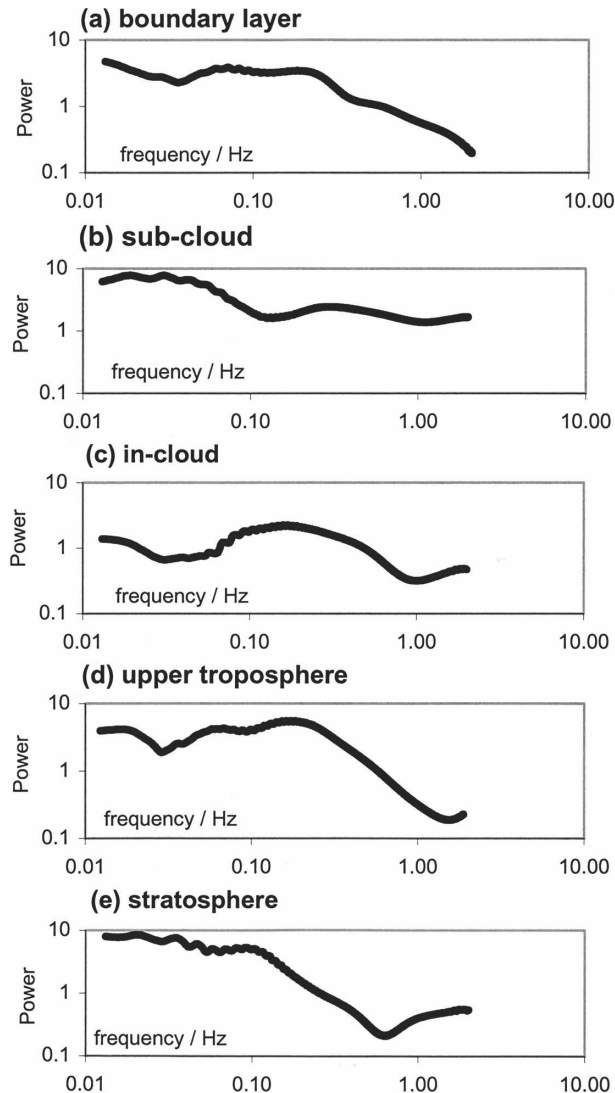
FIG. 4. Spectrum of variations obtained from a 100-s period of magnetic field data (a) in the boundary layer (decimal time 16.6 UTC), (b) subcloud (16.8 UTC), (c) in-cloud (17.1 UTC), (d) in the upper troposphere (17.5 UTC), and (e) in the stratosphere (17.7 UTC).

from nonturbulent to turbulent and then back to non-turbulent conditions. In Fig. 4b, there is a statistically significant ($p = 0.0025$) oscillation with period 43.6 s; in Fig. 4e there is an oscillation with period 37.1 s ($p < 0.001$). In the turbulent region (Fig. 4c), there are no such statistically significant peaks, implying that the motion is across a range of frequencies, and that slow oscillations, probably resulting from rotation slowly winding up the string and then unwinding, are not maintained.

Further information on the atmospheric structure at the same time as the ascent was available from the Chilbolton cloud radar. Figure 5 shows the cloud radar

parameters on the same day: the ice cloud base was at about 3 km. The turbulent dissipation rate ε ($m^2\,s^{-3}$) has also been derived, following the technique of Bouniol et al. (2003). Essentially, the radar makes high-resolution (1 Hz) measurements of the Doppler velocity at vertical incidence and its variance over a period of 30 s, which, coupled with a knowledge of the horizontal wind speed [from the model of the European Centre for Medium-Range Weather Forecasts (ECMWF)] to determine what scales are being sampled, allows ε to be estimated.

Above 4 km, the radar reflectivity factor exhibits a distinct fallstreak structure. The Doppler velocity indicates an ice particle fall speed of 0.5–1 $m\,s^{-1}$, superimposed on a gravity wave with an amplitude of up to 1 $m\,s^{-1}$. Below 4 km, the cloud structure is very different; latent cooling due to the evaporation of ice particles at cloud base causes convective instability in the form of narrow descending plumes of cloud (Harris 1977). Figure 5c shows the strong enhancement of turbulence at cloud base, contrasting with the much more quiescent air above 4 km.

Figure 6a shows the meteorological data obtained from the Reading balloon ascent, plotted as vertical profiles. Dewpoint variations show the top of the atmospheric boundary layer and the position of the base of the ice cloud, which was slightly higher than at Chilbolton.

Following the different time scales evident in Fig. 3c, the mean-squared change in the magnetic field measured by the Hall sensor was found, to allow detection of the rapid oscillations. Using 30-s blocks of data, the mean-squared difference in the magnetic field between adjacent 1-s samples was calculated. This parameter quantifies the rapidity of the oscillations and hence provides a measure of the intensity of the turbulence. It is preferable to the variance of the magnetic field in the 30-s period because, for oscillations with a period of less than 30 s, the variance alone would not indicate the rapidity of the oscillations. Figure 6b shows this quantity plotted as a vertical profile. It shows the strong signal of turbulence at the base of the cirrus, where the effect of evaporating ice particles at the base of ice clouds is known to generate turbulence (Harris 1977).

5. Conclusions

In this note we have demonstrated a promising technique to infer the intensity of atmospheric turbulence using an inexpensive balloon-borne Hall sensor. It adds little weight to an existing radiosonde launch, but permits additional information on the atmospheric structure to be retrieved. It could be developed further by
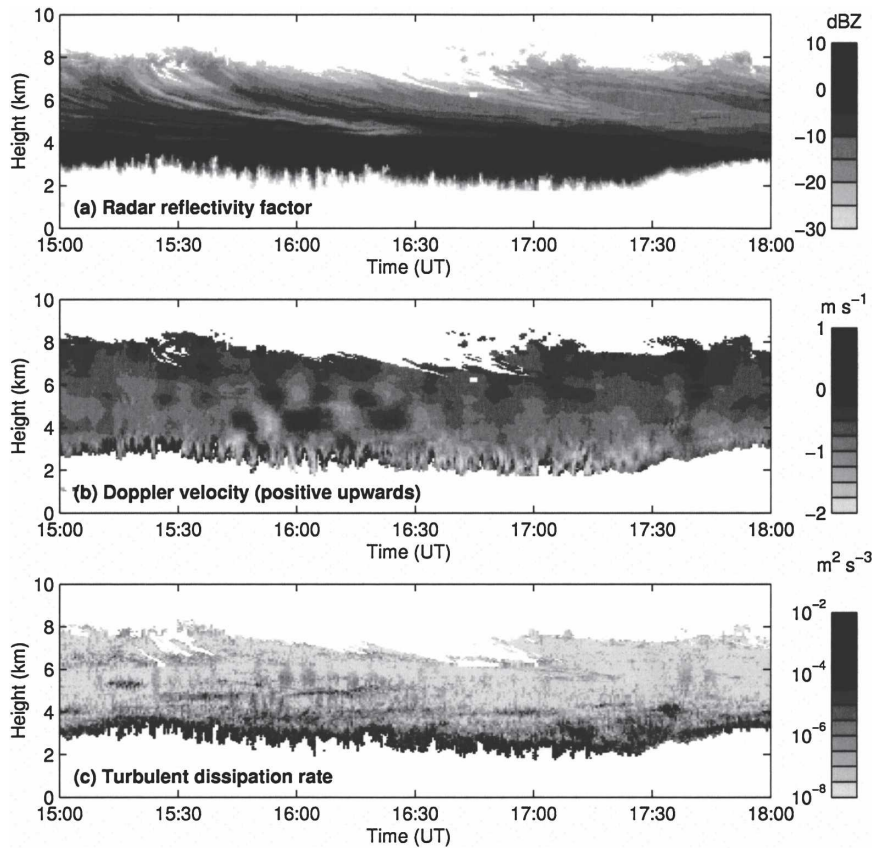
FIG. 5. Atmospheric properties sensed using the cloud radar at Chilbolton on 26 Jan 2004. Turbulent kinetic energy dissipation rate was derived using the technique of Bouniol et al. (2003).

employing a pair of Hall sensors to obtain the absolute two-dimensional orientation, and therefore the torque applied by the turbulent air. An important aspect is that, as the sensors are mounted within the radiosonde, and therefore that the device is not physically modified externally, no changes to the standard operational launch procedure are required: this may facilitate widespread use of this instrument.
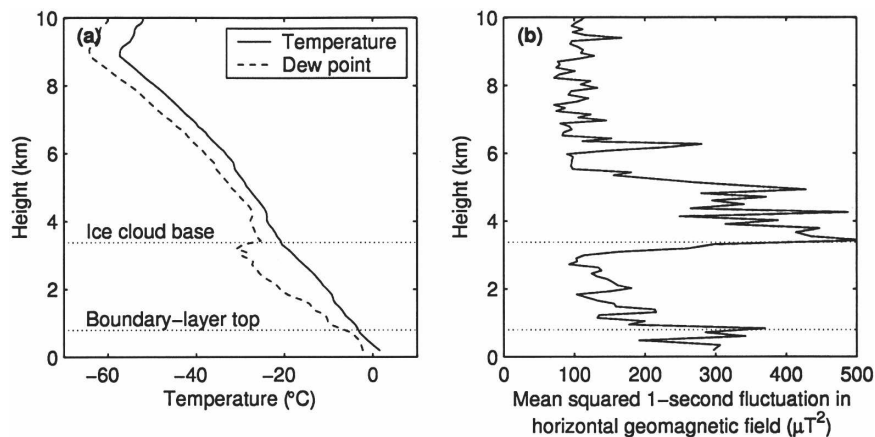

FIG. 6. Atmospheric radiosonde data acquired from 1638 UTC launch from Reading on 26 Jan 2004: (a) thermodynamic parameters; (b) mean-squared change in the magnetic field measured by the Hall probe, from one second to the next. (The Hall probe data were obtained at approximately 3 Hz and averaged to 30 s.)

REFERENCES

Bouniol, D., A. J. Illingworth, and R. J. Hogan, 2003: Deriving turbulent kinetic energy dissipation rate within clouds using ground based 94 GHz radar. Preprints, *31st Conf. on Radar Meteorology,* Seattle, WA, Amer. Meteor. Soc., 192–196.

Harris, F. I., 1977: The effects of evaporation at the base of ice precipitation layers: Theory and radar observations. *J. Atmos. Sci.,* **34,** 651–672.

Harrison, R. G., 2005: Inexpensive multichannel digital data acquisition system for a meteorological radiosonde. *Rev. Sci. Instrum.,* **76,** 026 103, doi:10.1063/1.1841971.

HMSO, 1961: *Handbook of Meteorological Instruments. Part II: Instruments for Upper Air Observations*. Meteorological Office, Her Majesty's Stationery Office, 209 pp.

MacCready, P. B., 1965: Comparison of some balloon techniques. *J. Appl. Meteor.,* **4,** 504–508.

MacGorman, D. R., and W. D. Rust, 1998: *The Electrical Nature of Storms*. Oxford University Press, 422 pp.

Maynaud, P. N., 1972: The aa indices: A 100 year series characterizing the magnetic activity. *J. Geophys. Res.,* **77,** 6870–6874.

Press, W. H., B. P. Flannery, S. A. Teukolsky, and W. T. Vetterling, 1992: Numerical Recipes in FORTRAN 77. Vol. 1., 2d ed., Cambridge University Press, 963 pp.